POX 186:
the ultracompact blue compact dwarf galaxy reveals its nature[*]

V. Doublier[1,2], **D. Kunth**[3], **F. Courbin**[4,5], **and P. Magain**[4]

[1] European Southern Observatory, Alonso de Cordova 3107, Casilla 19001, Santiago, Chile
[2] Observatoire de Marseille and Institut Cassendi, 2 place Le Verrier, 13004 Marseille, France
[3] Institut d'Astrophysique de Paris, 98bis Bld Arago, 75014 Paris, France
[4] Institut d'Astrophysique, Université de Liège, Avenue de Cointe 5, 4000 Liège, Belgium
[5] URA 173 CNRS-DAEC, Observatoire de Paris, 92195 Meudon Principal Cédex, France

Abstract. High resolution, ground based R and I band observations of the ultra compact dwarf galaxy POX 186 are presented. The data, obtained with the ESO New Technology Telescope (NTT), are analyzed using a new deconvolution algorithm which allows one to resolve the innermost regions of this stellar-like object into three Super-Star Clusters (SSC). Upper limits to both masses (M$\sim 10^5$ M$_\odot$) and physical sizes ($\leq$60pc) of the SSCs are set. In addition, and maybe most importantly, extended light emission underlying the compact star-forming region is clearly detected in both bands. The $R - I$ color rules out nebular Hα contamination and is consistent with an old stellar population. This casts doubt on the hypothesis that Blue Compact Dwarf Galaxies (BCDG) are young galaxies.

Key words: galaxies: compact – galaxies: distances and redshifts – galaxies: evolution – galaxies: formation – galaxies: photometry – galaxies: starburst

1. Introduction

Among the Blue Compact Dwarf Galaxy (BCDG) population, there exists a small class of very compact starforming objects, unresolved on photographic and CCDs images. This small fraction ($<$ 10%) of BCDGs does not appear to possess *any* underlying stellar component substantially older than the starburst population (Thuan (1983); Kunth et al. (1988); Drinkwater & Hardy (1991)). The most representative galaxy of this kind is the star-forming dwarf POX 186 (RA:13h23m12.0s; DEC:-11° 22'; B1950). This relatively nearby galaxy (recession velocity v = 1170 km s^{-1}) was discovered in a prism-objective survey search (Kunth et al. (1981)), and has been observed spectroscopically as part of a primordial He abundance study (Kunth & Sargent (1983)). Ground-based images taken at ESO

(Kunth et al. (1988)) revealed a nearly round, barely resolved object with no apparent substructure. The luminosity of this galaxy is about $M_V = -14$ (Kunth et al. (1988)) and population synthesis models predict that it should have a postburst luminosity as low as $M_V = -10$. Therefore, this object may represent the smallest unit of galaxy formation. Given POX 186's luminosity, its total luminous mass should be 10^8M$_\odot$ (H_0=80 km s^{-1} Mpc^{-1} and mass-to-light ratio of 1.). This exceeds by 1 to 2 order of magnitudes the mass of star clusters observed in our Galaxy or in neighboring galaxies.

It has been conjectured that POX 186 could be a young, isolated, giant star-forming cluster. The advent of HST, with its very high angular resolution, has permitted the discovery of so-called "Super-Star Clusters" (SSC) found in many starforming dwarf and irregular galaxies. One of the first and most remarkable examples is He2–10 by Conti & Vacca (1994) where UV images obtained with the Faint Object Camera on HST revealed 10 bright star clusters near the center of the galaxy as well as a large number of fainter clusters in a starburst region 8$''$ (350 pc) away from the center.

In this paper, we present optical observations obtained with the New Technology Telescope (NTT) at ESO, La Silla (Chile), and report on the presence of an extended faint halo underlying the starburst component. We show also that, using deconvolution, POX 186 can be resolved into several substructures which can be explained in terms of SSCs.

2. NTT observations

POX 186 was observed in the R and I bands at the NTT (ESO, Chile) with the SUperb Seeing Imager (SuSI) in February 1996. The pixel size of the detector is 0.128$''$. The weather conditions were photometric and the seeing was better than 0.9$''$. The exposures were split into two 10-minute exposures due to the high sky background.

The first part of the data reduction (i.e., bias subtraction and flat fielding using dome and sky flat-fields) was performed using the IRAF package. The cosmic-rays removal procedure available in MIDAS was applied to the images. As the scattered
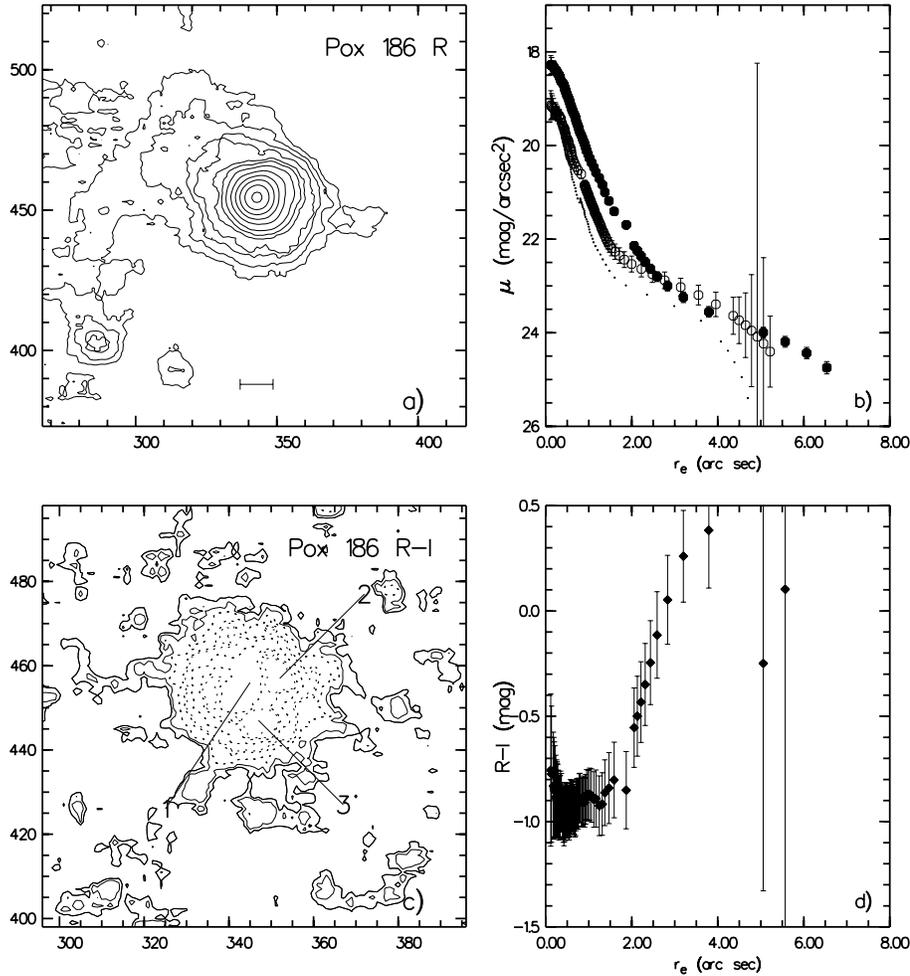

Fig. 1a–d. Surface photometry of POX 186. **a** An R band contour plot of POX 186, the size of the field is $18'' \times 18''$, North is up, and East is right. The contour interval is 0.5 mag. The lowest contour corresponds to a surface brightness of 24 mag arcsec^{-2}. The bar corresponds to a linear size of 100 pc (the linear scale is 71 pc/arcsec). **b** The light distribution profiles in R (filled circles) and I (open circles). The error bars on the light profiles have been computed assuming that Poisson statistics apply. The dotted profile corresponds to the R profile of a nearby non-saturated star. **c** A Contour plot of the $R - I$ map. The size of the field is $12'' \times 12''$. The **lowest** contour corresponds to a $R - I$ color of -0.8 mag **in the center of the galaxy**; the intervals between the contours are 0.1 mag, and the dashed contours represent negative values. **d** The $R - I$ color profiles, uncorrected for Galactic extinction. The errors are computed from the errors on the R and I profiles. Note the presence of 3 "blobs" on the $R - I$ map.

light from the moon caused an uneven sky-background around the galaxy, the sky was subtracted with a frame obtained by smoothing the reduced images with a median filter and a large smoothing box, while masking the objects in the frames. This was applied to each of the two frames which were then averaged.

2.1. Surface photometry

The photometric results are summarized in Table 1. This includes the asymptotic magnitude m$_{asym}$ (extrapolated integrated magnitude), the effective surface brightness μ_{eff} in mag/arcsec^2 (surface brightness at the half light radius), the effective radius r$_{eff}$ in arcseconds (half light radius) and the effective mean surface brightness $\langle \mu_{eff} \rangle$ (mag/arcsec^2) (mean surface brightness within r$_{eff}$), for the R and I bands. Finally, the scalelength parameter (α) and the central surface brightness (μ_0) derived by extrapolating the fit at the equivalent radius to zero, are given.

The errors on the integrated magnitudes are 0.05 mag in both the R and I bands. Errors on the surface brightness measurement were computed assuming that Poisson statistics applied.

A $18'' \times 18'' R$ band contour plot centered on POX 186 is shown in Fig. 1a. The bar indicates a linear size of 100 pc

Table 1. Photometric results for POX 186

	R	I
m$_{asym}$	16.36	17.05
μ_{eff}	22.23	21.52
r$_{eff}$	3.75	2.35
$\langle \mu_{eff} \rangle$	21.20	20.90
μ_0 (exp)	22.03 (0.04)	21.68 (0.01*)
μ_0 (r$^{1/4}$)	13.52 (0.21)	13.23 (0.08)
α (kpc^{-1})	5.56 (0.72)	6.14 (0.40)

* 1-σ error

(H$_0$ = 80 km s^{-1} Mpc^{-1}). The surface brightness profiles in the R band (filled circles) and I band (open circles) are displayed in Fig. 1b. The $R - I$ color map ($12'' \times 12''$), and the color distribution profile as a function of the equivalent radius (De Vaucouleurs & Aguero (1973)) are displayed in Figs. 1c and 1d, respectively.

A more detailed explanation of the surface photometry and color distribution profiles is given in Doublier et al. (1997).

2.2. Images and light distribution profiles

POX 186 is clearly resolved (see Fig. 1a) in our sub-arcsecond images (r$_{eff}$(R) = 3.75'', r$_{eff}$(I) = 2.35''). An obvious asym-

metry in the external isophotes can be seen on the Eastern side of the nucleus. It is seen in both our R and I band images. Two different regions are seen on the $R - I$ color plot (Fig. 1d). While the innermost region of the galaxy is blue ($R - I \sim -0.8$), the outer part shows a red color gradient. Over a region extending from $2''$ to $6''$ (i.e., over about 280 pc) away from the nucleus, the $R - I$ color increases from –0.8 mag to 0.4 mag. This color distribution translates into a color gradient of ~ 4.2 mag/kpc.

Furthermore, the $R - I$ map (Fig. 1b) reveals three distinct substructures in the central parts of the galaxy (labelled "1", "2", "3"), the largest of them being centered with respect to the outer isophotes. This suggests that the central nucleus, which was originally thought to be single, consists of smaller units.

Alternatively, the observed structures could be due to signal fluctuations due to poor alignment of the frames. Such an effect would be enhanced when creating the color maps. However, other objects (stars) do not show such artifacts. We can therefore safely consider these structures to be real and intrinsic to the galaxy.

We used the algorithm developed by Saglia et al. (1997) to fit the light distribution profiles in the R and I bands. The central parts of the two profiles are not well fitted by a $r^{1/4}$ law. A model that includes an exponential profile and an $r^{1/4}$ gives a better fit to the data; however, the best fit still leaves significant residuals in the center of the frame. This suggests that POX 186 is not a single spheroidal object, like a large star cluster. On the contrary, the galaxy appears to be composed of a nucleus with a profile broader than a $r^{1/4}$ law, plus underlying emission compatible with an exponential profile.

Fig. 2. *Top panels* show the reduced R and I band frames. *Middle* and *bottom panels* show the result of the deconvolution with different intensity cuts.

3. Underlying galaxy and starburst

The extended features observed in the R and I frames and "knotty" center of the $R - I$ map have been deconvolved with a new deconvolution algorithm developed by Magain et al. (1998). The algorithm decomposes the images into a sum of point sources plus a diffuse deconvolved background smoothed on a length scale *chosen by the user*. As output, the program returns the photometry and position of the point sources, as well as a deconvolved image.

The main idea behind the new deconvolution technique, is to avoid deconvolution by the total Point Spread Function (PSF) of the image, Instead, a narrower function is used, allowing the spatial frequencies of the deconvolved image to stay within the limits imposed by the sampling theorem. As a consequence, most of the so-called "deconvolution artifacts" are avoided.

The good sampling of the images (pixel size of $0.128''$) and the good stability of the PSF across the field make our data well suited for deconvolution. The FWHM in the undeconvolved images is of the order of $0.85''$. The deconvolved images have a resolution of $0.38''$. This is dictated by the signal-to-noise of our data. The PSF needed for deconvolution was obtained from a star, about as bright as POX 186 and situated $1'$ away.

We consider that the solution found by the deconvolution procedure is good when the residual map, in units of the photon noise, has the correct statistical distribution across the whole
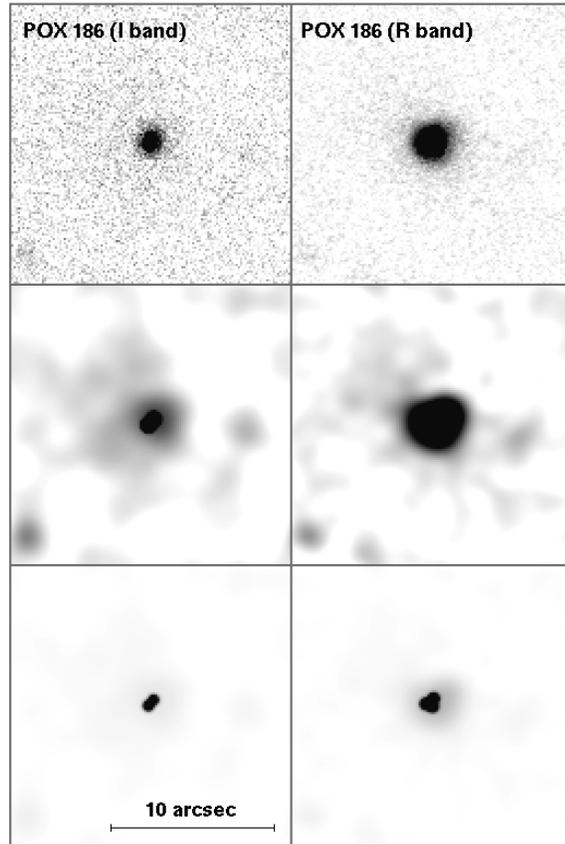
field, i.e. equal to one (or very close, see Courbin et al. (1998) and Burud et al. (1998) for more details on this procedure).

The residual maps obtained show significant structures when only one point source is used to model the center of POX 186. A second point source was added to obtain good residual maps in the I band, whereas a third source had to be used to fit properly POX 186's nucleus in the R band. Note that adding more point sources leads to over-fitting the central parts of the galaxy. We can therefore conclude that the present data are compatible with a galaxy nucleus composed of 3 point sources in R and at least 2 in I.

Fig. 2 shows the R and I band images with different cut-off intensity in order to display better either the faint extensions of the galaxy, or the bright central region. While the diffuse halo of the galaxy was already detected in the reduced R band frame (S/N > 3), it is hardly seen in the I frame (S/N $\leq$ 3) despite an obvious asymmetry of the image. This diffuse halo clearly shows up on the surface brightness profiles, where we can reach brightness levels as faint as a few percent of the sky background level. The diffuse halo can also be seen in the deconvolved images.

From the deconvolved images, we obtained an estimate of the luminosity and the masses of the "clusters" (Table 2). Because of the limited S/N ratio and the heavy blend-

Table 2. Derived luminosities and masses of the deconvolved clusters

N^o	m	R M$_R$	Mass*	m	I M$_I$	Mass*
1	19.23	−11.59	2.3	19.61	−11.21	1.2
2	19.27	−11.55	2.2	19.85	−10.97	0.9
3	19.47	−11.35	1.8	not	detected	−

* Mass in units of 10^6 M$_\odot$

ing of the knots, the magnitude errors are large, about 0.5 mag. The absolute magnitudes are computed assuming $H_0 = 80\,\mathrm{km\,s^{-1}\,Mpc^{-1}}$, and the masses are determined by assuming a mass-to-light ratio of 1 (recent HI observations of POX 186 set an upper limit of a few 10^6 M$_\odot$, S. Coté, private communication). The masses are large compared with the observed masses of single SSCs (Meurer et al. (1995)). However, if the mass-to-light ratio estimates of Charlot et al. (1996) for a single burst stellar population of age less than 10^7 years ($M/L = 0.1 M_\odot/L_\odot$) are more realistic, the "clusters" in POX 186 will have smaller masses (10^4 to 10^5 M$_\odot$). This is similar to those of SSCs observed in other starburst galaxies.

The physical sizes of the knots are difficult to ascertain. They are unresolved and the only constraint we can set on their size is given by the seeing of the observations, 0.85″, or about 60 pc. Their size on the deconvolved image, 0.384″ (about 26 pc) only reflects the adopted resolution limit.

As a check on the accuracy of the deconvolution, we also generated the two-dimensional cross-correlation map of the R and I band "un-deconvolved" frames (Fig. 3). Only the levels above 0.5 are displayed in Fig. 3 (a level of 0. implies no correlation and a level of 1. implies full correlation). The cross-correlated image reproduces very well the structures seen in both deconvolved frames. This indicates that they are real and that they are not due to noise enhancement introduced by poor sky subtraction, or by the deconvolution process.

One of the knots in R is not detected in the I band, although the cross-correlation map shows an obvious asymmetry at the corresponding position on the R frame. The residual maps after deconvolution in R, are significantly better when three point source are considered. Detecting only two of them in the I band may therefore indicate that the third is too faint. Indeed, the I band magnitude of the counterpart of the "missing" knot would be about 20 mag. which is still consistent with the central $R - I$ index of –0.8.

The extended component of POX 186 shows a filamentary structure instead of a smooth light distribution as usually seen in BCDGs (Papaderos et al. (1996), Telles et al. (1997), Doublier et al. (1997)). Although this is at the limit of the noise level of the present data, the filaments can be seen in both the deconvolved images and the cross-correlation map. The low surface brightness component of POX 186 may be similar to the filamentary structures seen in dwarf irregulars, rather than the smoother surface profiles of BCDGs.
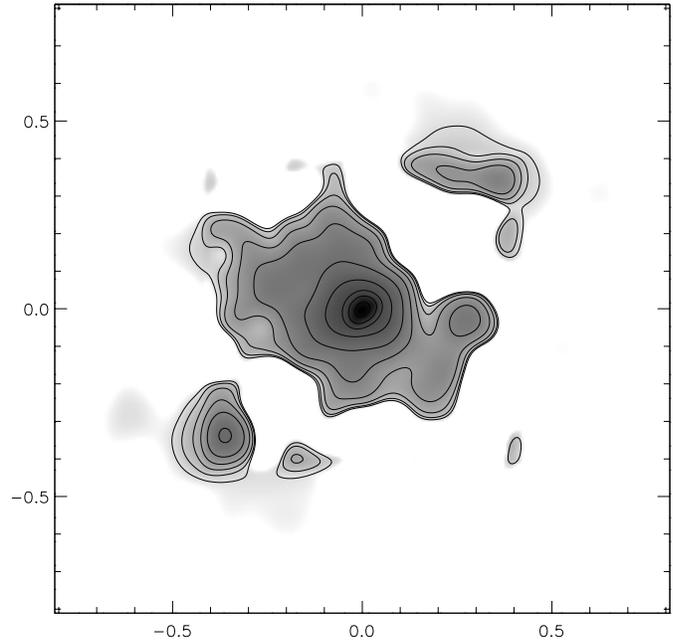

Fig. 3. Two-dimensional cross-correlation map for the R and I frames. The grey levels increase from 0. (no correlation, white) to 1. (exact correspondence, black). The contours are levels above 0.5, and the step between contours is 0.05

Further observations in the near-IR with high-sensitivity detectors and larger telescopes (the expected surface brightness of an evolved stellar population in K band is below 21 mag. arcsec^{-2}, i.e., the limit for 4 meter-class telescope with the current detectors) will elucidate the nature of the stellar population in this "halo".

4. Discussion

4.1. Nature of the galaxy

We have shown that the faint halo seen around the nucleus of POX 186 is a real structure, rather than an artefact produced by sky background subtraction, or by the deconvolution.

The nature of this diffuse component could be due to an evolved stellar population, or to Hα emission contaminating the R band, leaking from the star forming region. However, if the extension was due to Hα emission, the I band profile would not be so similar. Moreover, the $R - I$ color distribution would not exhibit a steep color gradient. Its observed apparent increase is in fact due to a decrease of the contribution of the R band flux with respect to the I band. This is definitely not consistent with the contamination hypothesis of the R band by Hα at large radii.

From the previous observations, no underlying component was detected, and it was argued that the red colors obtained by Kunth et al. (1988) ($B - R = 1.28$) were due to Hα emission contaminating the R band filter. However, together with the $B - R$ color, the $R - I$ color of the faint extension is consistent with emission dominated by red giant stars of spectral type G (Johnson (1966)). From the observed emission-line ratios, we know that internal reddening is negligible, so that the $R - I$
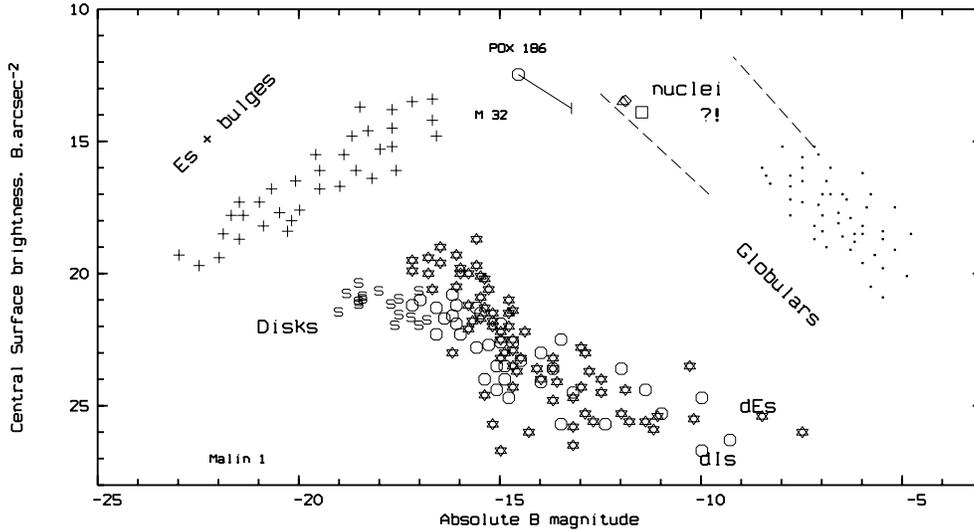
Fig. 4. [μ_0, M_B] plane: elliptical galaxies and bulges of spirals are represented as crosses, spiral disks as "s", dwarf galaxies as open symbols: stars for dwarf ellipticals and open circles for dwarf irregulars, globular clusters are represented as points. POX 186 is placed twice: the open circle corresponds to [μ_0, M_B] for total galaxy, the triangle and the square represent the clusters detected in the deconvolved images.

color cannot be attributed to dust. There is therefore strong evidence for an extended faint component of old stars underlying a starburst region.

4.2. POX 186 among the other dwarf galaxies population

POX 186 is a very small and compact object compared with other BCDGs: its effective radius is less than 300 pc in R, and less than 200 pc in I, while the mean effective radius (R band) for a typical BCDG is about 800 pc (Doublier et al. (1997); Doublier et al. (1999)). The compactness index (ratio of the effective radius to the radius at 1/4th of the total luminosity) of POX 186 is $r_{0.5}/r_{0.25} = 3.3$ in R; the mean compactness index value for BCDGs is 2.3 (Doublier et al. (1999)). It is 1.78 in the I band. This indicates that the galaxy is much less compact in I than in R, supporting the hypothesis of the presence of an extended structure underlying the starburst component. This compares well with irregular galaxies which have compactness indexes of 1.6, whereas elliptical galaxies have larger compactness indexes of 2.9–3.0 (Fraser (1977); De Vaucouleurs & Aguero (1973)).

Using the $B - R$ color given by Kunth et al. (1988) to estimate a lower limit for the central surface brightness $\mu_0(B)$ in the B band, we can place POX 186 in the diagram [μ_0, M_B] derived by Binggeli & Cameron (1991). POX 186 is located in the continuation of the sequence defined by elliptical galaxies and spiral bulges. The exponential underlying component is located within the sequence defined by the dwarf irregulars and disks of spirals in the [μ_0, M_B] plane. In the [$\log(\alpha)$, M_B] diagram, the underlying component falls well below the bulk of dEs, dIS and S0s. It is therefore more likely to be associated to Low Surface Brightness galaxies than to dwarf irregulars.

The 3 "clusters" lie well within the "galactic nuclei" sequence discussed by Binggeli & Cameron (1991) and Phillips et al. (1996), in the [μ_0, M_B] plane. In addition, population synthesis evolutionary models predict that the star forming regions fade considerably following an instantaneous burst (about 3–5 magnitude in the B band; Cerviño & Mas-Hesse (1994)). If we apply the predicted dimming to the 3 clusters, they evolve to the Globular Cluster sequence in the [μ_0, M_B] plane.

5. Conclusion

The primary result of our study is the detection of an extended faint component of old stars.

As revealed by optical CCD imaging, most BCDGs show a faint envelope surrounding the compact central starburst region (Thuan (1983); Hunter & Gallagher (1985); Kunth et al. (1988)). Near-infrared observations and evolutionary synthesis models have shown that these faint envelopes are composed of stars older than several Gyrs (Thuan (1983); Hunter & Gallagher (1985); Doublier et al. (1999)). However, any previous major episode of star formation must have been rather mild since the large value of the Hβ equivalent width (370 Å) observed in the very center of POX 186 (Kunth & Sargent (1983)) indicates that the underlying component does not contribute enough to the optical continuum so as to dilute significantly the emission line. Moreover, the optical spectrum shows a very high excitation and the overall measured metallicity is low ($Z \sim Z_\odot/10$, Kunth & Sargent (1983)). Using a closed-box model for chemical enrichment, the present burst could account for most of the metal enrichment and continuum light (Marconi et al. (1994)). No HI has been detected in POX 186. It could be that it has been exhausted. Alternatively, the gas could have been highly ionized and/or dispersed by the strong winds generated by the massive stars in the clusters.

Our second result is the discovery of Super Star Clusters (SSCs) in POX 186. The deconvolution technique reveals the presence of at least two "clusters" in the center of POX 186, with properties similar to that of the SSCs observed by Meurer et al. (1995) in other starburst galaxies. They found SSCs in HST FOC UV images of a sample of nine starburst galaxies. The SSCs in their sample account for about 20% of the total observed UV flux. Similar SSCs have been discovered in several other irregular or starburst galaxies (e.g., NGC 1569, NGC 1705: O'Connell et al. (1994); NGC

1140: Hunter et al. (1994); M82: O'Connell et al. (1995); NGC 4214: Leitherer et al. (1996); NGC 253: Watson et al. (1996)). These clusters have luminosities in the range $-14 < M_V < -11$, diameters of the order of 10 pc or less, and estimated masses in the range $10^4 - 10^6$ $M_\odot$ (e.g., Hunter et al. (1994); O'Connell et al. (1994); Conti & Vacca (1994)). Typical sizes and upper-mass estimates of SSCs are consistent with those of Galactic globular clusters and it is suggested that these SSCs may be globular clusters in the process of formation, with ages of less than 10^7 yrs (Conti & Vacca (1994)). At this point, we remark upon the work by Phillips et al. 1996 based on the nuclei and "knots" of late-type galaxies. They find an obvious overlap in properties between the large star clusters in these galaxies and the nuclei. Current discussions aim at establishing whether stellar-like cusps could be remnants of a previous starburst episode (Kormendy (1989)). We believe that the multiple sources observed in POX 186 could be SSCs like in other starbursting galaxies. Their derived absolute magnitudes agree well with those of SSCs observed in starburst galaxies. Clearly, it is mandatory to confirm the existence of the substructures in POX 186: SSCs and underlying galaxy. First, POX 186 remains one of the smallest star-forming galaxy: the exponential scale length of POX 186 (< 200 pc) is small compared to other known BCGDs. Second, the presence of SSCs raises new questions about its future evolution. Finally, the presence of the underlying old component removes POX 186 from the "young" galaxy candidates list.

References

Binggeli B., Cameron L. M., 1991, A&A 252, 27
Burud I., Courbin F., Lidman C., et al., 1998, ApJ 501, L5
Cerviño M., Mas-Hesse J. M., 1994, A&A 284, 749
Charlot S., Worthey G., Bressan A., 1996, ApJ 457, 625
Conti P. S., Vacca W. D., 1994, ApJ 423, L97
Courbin F., Lidman C., Frye B. L., et al., 1998, ApJ 499, L119
De Vaucouleurs G., Aguero E. L., 1973, PASP 85, 150
Doublier V., Caulet A., Comte G., 1999, submitted A&A
Doublier V., Comte G., Petrosian A., Surace C., Turatto M., 1997, A&AS 124, 405
Drinkwater M., Hardy E., 1991, AJ 101, 94
Fraser C. W., 1977, A&AS 29, 161
Hunter D. A., Gallagher J. S. I., 1985, AJ 90, 1457
Hunter D. A., O'Connell R. W., Gallagher John S. I., 1994, AJ 108, 84
Johnson H. L., 1966, ARA&A 4, 193
Kormendy J., 1989, ApJ 342, L63
Kunth D., Sargent W. L. W., 1983, ApJ 273, 81
Kunth D., Maurogordato S., Vigroux L., 1988, A&A 204, 10
Kunth D., Sargent W. L. W., Kowal C., 1981, A&AS 44, 229
Leitherer C., Vacca W. D., Conti P. S., et al. 1996, ApJ 465, 717
Magain P., Courbin F., Sohy S., 1998, ApJ 494, 472
Marconi G., Matteucci F., Tosi M., 1994, MNRAS 270, 35
Meurer G. R., Heckman T. M., Leitherer C., et al., 1995, AJ 110, 2665
O'Connell R. W., Gallagher John S. I., Hunter D. A., 1994, ApJ 433, 65
O'Connell R. W., Gallagher John S. I., Hunter D. A., Colley W. N., 1995, ApJ 446, L1
Papaderos P., Loose H. H., Fricke K. J., Thuan T. X., 1996, A&A 314, 59
Phillips A. C., Illingworth G. D., Mackenty J. W., Franx M., 1996, AJ 111, 1566
Saglia R. P., Bertschinger E., Baggley G., et al., 1997, ApJS 109, 79
Telles E., Melnick J., Terlevich R., 1997, MNRAS 288, 78
Thuan T. X., 1983, ApJ 268, 667
Watson A. M., Gallagher J. S. I., Holtzman J. A., et al., 1996, AJ 112, 534